J. Fluid Mech. (1993), *vol.* 247, *pp.* 527–549

Copyright © 1993 Cambridge University Press

On the 'δ-equations' for vortex sheet evolution

By JAMES W. ROTTMAN[1] AND PETER K. STANSBY[2]

[1] Universities Space Research Association, NASA/Goddard Space Flight Center, Greenbelt, MD 20771, USA

[2] Department of Engineering, Simon Building, The University, Manchester M13 9PL, UK

(Received 11 July 1991 and in revised form 11 September 1992)

We use a set of equations, sometimes referred to as the 'δ-equations', to approximate the two-dimensional inviscid motion of an initially circular vortex sheet released from rest in a cross-flow. We present numerical solutions of these equations for the case with $\delta^2 = 0$ (for which the equations are exact) and for $\delta^2 > 0$. For small values of the smoothing parameter δ a spectral filter must be used to eliminate spurious instabilities due to round-off error. Two singularities appear simultaneously in the vortex sheet when $\delta^2 = 0$ at a critical time t_c. After t_c the solutions do not converge as the computational mesh is refined. With $\delta^2 > 0$, converged solutions were found for all values of δ^2 when $t < t_c$, and for all but the two smallest values of δ^2 used when $t > t_c$. Our results show that when $\delta^2 > 0$ the vortex sheet deforms into two doubly branched spirals some time after t_c. The limiting solution as $\delta \to 0$ clearly exists and equals the $\delta = 0$ solution when $t < t_c$. For $t > t_c$, the limiting solution appears to exist if only the converged solutions are used, but it is unclear what relation this limiting solution has to any $\delta^2 = 0$ solution for these times.

1. Introduction

The numerical solution of the equations describing the solution of a two-dimensional vortex sheet embedded in an ideal fluid has proved to be a very challenging problem. Most numerical methods appear to produce reasonable results when modest values of the parameters describing the computational mesh are used, but produce irregular or inconsistent results as the computational mesh is refined; that is, the discretizations of the equations describing vortex sheet motion apparently fail to converge. Recently, Krasny (1986*a*) has summarized the previous numerical attempts at solving these equations and has concluded that they have failed for two fundamental reasons.

The first reason is that round-off error introduces spurious perturbations into the calculations that, due to the intrinsic susceptibility of vortex sheets to Helmholtz instability, grow rapidly to destroy the accuracy of the calculations. Krasny (1986*a*) has shown that these spurious instabilities can be suppressed either by increasing the arithmetic precision as the computational mesh is refined or, more practically, by applying a spectral filter at each time step to eliminate wavenumbers whose Fourier coefficients' amplitudes are less than the round-off error. Using these techniques, Krasny (1986*a*) produced convincing results that for times less than a finite critical time t_c the point-vortex method for computing the rollup of a periodically perturbed flat vortex sheet converged as the number of vortices used to describe the sheet was increased.

The second reason is that apparently the exact solution develops a singularity at some point on the vortex sheet at t_c. The asymptotic analysis of Moore (1979) and

the numerical evidence produced by Meiron, Baker & Orszag (1982), Krasny (1986*a*) and Rottman, Simpson & Stansby (1987) suggest that the vortex sheet becomes non-analytic at t_c. In general, the vortex sheet's curvature becomes infinite at some point where the vorticity distribution has formed a cusp, although the sheet remains continuous. Presumably, numerical methods fail to converge after the critical time because their differencing schemes become inconsistent when the solution becomes non-analytic.

The appearance of a singularity at a finite critical time raises several intriguing questions. Does a solution exist for $t > t_c$ and if so is it unique and how can it be computed? In an attempt to gain some insight into these questions, Krasny (1986*b*, 1987) applied a refinement of a method originally proposed by Anderson (1985) to compute the rollup of a vortex sheet before and after t_c. Krasny replaced the exact equations governing vortex-sheet motion with desingularized approximate equations that he refers to as the 'δ-equations', which reduce to the exact equations in the limit as the smoothing parameter δ vanishes. When discretized by approximating the vortex sheet by a finite number of points, these approximate equations become the 'vortex blob' method introduced by Chorin & Bernard (1973) and in the limit as $\delta \to 0$ this method reduces to the point-vortex method first used by Rosenhead (1931). These desingularized equations have better behaved solutions than the exact equations and therefore are more tractable for numerical calculation. Anderson proposed that some insight into the nature of the solutions of the exact equations may be obtained by studying the limit of the solutions of the approximate equations as $\delta \to 0$.

Although the solutions of the δ-equations are better behaved than those of the exact equations, the approximate solutions for small δ are susceptible (although less severely) to spurious instabilities due to round-off error. Krasny's refinement of Anderson's method is to incorporate spectral filtering to eliminate these spurious instabilities. He applied this technique to the rollup of a periodically perturbed vortex sheet (Krasny 1986*b*), and to the rollup of vortex sheet behind an aircraft wing (Krasny 1987). In both cases he produced numerical results that suggest the limit of the converged approximate solutions exists as $\delta \to 0$ for times both before and after t_c, even though the solutions of the exact equations converge only for times before t_c. The limiting approximate solution indicates that the vortex sheet deforms into a spiral with an infinite number of turns centred at the point where a singularity forms in the exact solution at t_c, although it is not clear in what sense this limiting solution is a solution of the exact equations.

Krasny has emphasized that his work on the convergence of vortex-sheet methods is primarily of an experimental nature. The rigorous mathematical foundation for this problem, although developing rapidly in the last few years, is still incomplete. The existence of solutions of the exact equations for vortex sheets with analytic initial conditions has been proved for short times by Sulem *et al.* (1981), and for times up to nearly the time of singularity formation by Caflisch & Orellana (1986). For certain kinds of non-analytic initial conditions, Ebin (1988) and Caflisch & Orellana (1989) have proved that the vortex-sheet problem is ill-posed. Although Caflisch & Lowengrub (1989) have proved the convergence of the point-vortex and vortex-blob methods for small analytic perturbations of a planar vortex sheet, their proof is restricted to small times and certainly does not extend to the time at which vortex-sheet rollup begins.

Recently, Tryggvason, Dahm & Sbeih (1991) have compared solutions of the δ-equations with numerical solutions of the fully viscous Navier–Stokes equations for

the rollup of initially planar thin vortex layers at high Reynolds numbers. They found that the solutions of the δ-equations accurately reproduce only the large-scale features of rollup for vorticity layers of finite initial thickness. However, their results indicate that the limits of the solutions as δ goes to zero for the inviscid problem and as the initial thickness of the vortex layer approaches zero for the viscous problem at high Reynolds number are the same.

In the present paper we describe an attempt to use Krasny's method to study the rollup of a vortex sheet that represents the boundary of cylinder of a fluid released from rest in a steady cross-flow. This problem has been studied earlier by Rottman *et al.* (1987) using a vortex-sheet method. They estimated the critical time, computed the rollup of the vortex sheet with $\delta = 0.1 r_0$ (where r_0 is the initial radius of the circle) and estimated the large-time steady-state flow. However, they did not study the detailed structure of the singularity that forms at the critical time nor the behaviour of the vortex rollup in the limit as $\delta \to 0$. We present here a detailed numerical study of the structure of the singularity that forms when $\delta^2 = 0$ and of the vortex rollup when $\delta^2 > 0$. We also discuss some difficulties we encountered in attempting to obtain the limit of the solution as $\delta \to 0$ when $t > t_c$.

2. Problem formulation

The initial-value problem under consideration is sketched in figure 1. We consider the two-dimensional motion of a vortex sheet with initially circular cross-section of radius r_0 embedded in an unbounded ideal fluid. The initial conditions are that of potential flow outside the vortex sheet with uniform speed U_0 at infinity and that of a state of rest inside the vortex sheet.

Following Anderson (1985) and Krasny (1986*b*), we will use the following approximate form (sometimes referred to as the δ-equations) of the equations governing the motion of the vortex sheet:

$$\frac{\partial z^*}{\partial t} = U_0 + \frac{1}{2\pi \mathrm{i}} \oint \frac{(z-z')^* \gamma(\xi')}{|z-z'|^2 + \delta^2} \mathrm{d}\xi', \tag{2.1}$$

where $z(\xi, t) = x(\xi, t) + \mathrm{i}y(\xi, t)$ is the complex coordinate (all other quantities are real) for a point on the vortex sheet specified by the Lagrangian parameter ξ and the time t. We have used the notation $z' \equiv z(\xi', t)$ and $z^* \equiv x - \mathrm{i}y$. The vortex-sheet strength per unit ξ is denoted as $\gamma(\xi)$, and in this formulation γ is independent of time. What makes these equations approximate is the presence of the smoothing parameter δ, which has the dimension of length. The exact equations for the motion of a closed vortex sheet are recovered by setting $\delta = 0$ and interpreting the integral in (2.1) as its Cauchy principal value.

We define ξ to be the initial angular position of a point on the vortex sheet. Then the initial condition for z is

$$z(\xi, 0) = r_0 \exp(\mathrm{i}\xi), \tag{2.2}$$

and we specify

$$\gamma(\xi) = -2U_0 r_0 \sin(\xi). \tag{2.3}$$

This last condition produces the exact initial motion only when $\delta^2 = 0$, since (2.1) is an approximate expression for the vortex sheet motion when $\delta^2 > 0$.

To solve numerically the problem formulated by (2.1)–(2.3) with $\delta^2 > 0$, we divided the vortex sheet into N points with coordinates (x_j, y_j) at equally spaced values of the Lagrangian parameter $\xi_j = (j - \frac{1}{2}) 2\pi/N$, where $j = 1, 2, \ldots, N$. Then, with the

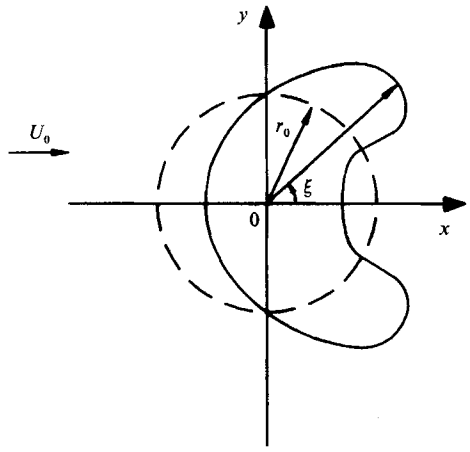

FIGURE 1. A definition sketch of the flow. The dashed line represents the initial shape of the vortex sheet and the solid line is the vortex sheet at some later time.

integrals in (2.1) approximated by the trapezoidal rule, we obtain the following set of $2N$ ordinary differential equations:

$$\frac{dz_j^*}{dt} = U_0 + \frac{1}{2\pi i} \sum_{\substack{k=1 \\ k \neq j}}^{N} \frac{(z_j - z_k)^* \Gamma_k}{|z_j - z_k|^2 + \delta^2}, \tag{2.4}$$

where $\Gamma_j = \gamma(\xi_j)\, 2\pi/N$. These are the 'vortex blob' equations originally introduced by Chorin & Bernard (1973). Since z is a periodic function of ξ, this discretization of (2.1) has a spatial truncation error that decreases exponentially with increasing N, provided $\delta^2 > 0$ and $z(\xi, t)$ remains analytic.

To advance the calculation in time, we used a standard fourth-order Runge–Kutta scheme with a fixed time step Δt. Tests showed that this scheme had the expected temporal truncation error that behaved as $(\Delta t)^4$. As a check on the accuracy of the time integration scheme, the value of the Hamiltonian function

$$H = \sum_{j=1}^{N} \sum_{k=j+1}^{N} \Gamma_j \Gamma_k \log\left(|z_j - z_k|^2 + \delta^2\right) \tag{2.5}$$

was monitored. This function is an invariant of the spatially discrete equation (2.4) with $\delta^2 \geqslant 0$. In all the calculations described in this paper using equations (2.4), the time step Δt was chosen small enough so that H was conserved to within a specified accuracy.

When $\delta^2 = 0$, the integrand in (2.1) is singular at $\xi' = \xi$ and the discretization (2.4) is no longer exponentially accurate. Equations (2.4) with $\delta^2 = 0$ are equivalent to Rosenhead's (1931) original point-vortex approximation. A more accurate discretization is the following, which we refer to as the vortex-sheet method:

$$\frac{dz_j^*}{dt} = U_0 + \frac{1}{2\pi i}\left\{ \sum_{\substack{k=1 \\ k \neq j}}^{N} \frac{(z_j - z_k)^* \Gamma_k}{|z_j - z_k|^2} - \left(\frac{d\Gamma}{d\xi} \Big/ \frac{\partial z}{\partial \xi}\right)_{\xi = \xi_j} + \tfrac{1}{2}\Gamma_j \left[\frac{\partial^2 z / \partial \xi^2}{(\partial z/\partial \xi)^2}\right]_{\xi = \xi_j} \right\}. \tag{2.6}$$

The last two terms in (2.6) are the contributions to the integral in (2.1) of the singular integrand near $\xi' = \xi$. These correction terms were first introduced into vortex-sheet theory by van de Vooren (1980) for an infinitely long vortex sheet and were shown to apply also to closed vortex sheets by Moore (1981). If the derivatives in the

correction terms are evaluated using a spectral method, then the spatial truncation error of this discretization decreases exponentially with increasing N (again, provided that $z(\xi, t)$ remain analytic).

The point-vortex method is equivalent to using (2.6) with van de Vooren's correction terms neglected. As shown by Moore (1981), this means that the point vortex method has a spatial truncation error that decreases as $1/N$, which is substantially slower convergence than that of the vortex-sheet method. Consequently, in the limit as $\delta \to 0$ in (2.4) a much larger number of points must be used to achieve the same spatial accuracy as would be obtained by the use of (2.6).

We found that for small values of δ the calculations using (2.4) developed an instability which became more severe as N was increased. The same instability occurred when we used (2.6). We removed this instability by filtering the solution to eliminate spurious perturbations introduced by round-off errors. The filter is analogous to that suggested by Krasny (1986*a*, *b*) in which after each time step the z_j are fast Fourier transformed and all the Fourier coefficients with magnitudes less than some small value ϵ were set to zero before synthesis. Krasny recommended setting ϵ equal to the machine arithmetic precision and we found that this was generally adequate. The use of this filter prevents the occurrence of spurious instabilities, but it also introduces a systematic error that depends on the value of ϵ and the size of the time step. Pugh (1989) noted that for very small time steps the filter prevents any growth of the solution, because the time step is too small for the 'true' solution to increase even as much as ϵ. So far, there has been no rigorous analysis of the error introduced by the filtering technique, so the choice of ϵ and the time step that suppresses the spurious instabilities and introduce the minimum error have to be found by trial and error.

In the remaining sections of this paper we make all variables non-dimensional with r_0 as the lengthscale and r_0/U_0 as the timescale.

3. Numerical results with $\delta^2 = 0$

Here we summarize the results for the problem formulated in the previous section with $\delta^2 = 0$. This problem was considered previously by Rottman *et al.* (1987) using a slightly different vortex-sheet formulation than described in the previous section. They found that the calculation developed a sawtooth instability at some critical time t_c. This critical time was estimated to be $t_c \approx 0.55$ in the limit $N \to \infty$, where N is the number of points describing the vortex sheet. At the critical time the vortex sheet was smooth and only slightly distorted from its initially circular shape, but a closer look at the results revealed that the curvature had become infinite and the vorticity strength per unit arclength had formed a cusp at two points on the sheet. These two points were located symmetrically about the x-axis on the downstream side of the vortex sheet.

We have recomputed this problem using the vortex-sheet method outlined in the previous section. The main differences between the present method and that used by Rottman *et al.* (1987) are the time integration scheme and the markers used to follow the motion of the vortex sheet. As explained earlier, we use a fourth-order Runge–Kutta scheme with a fixed time step whereas Rottman *et al.* used a variable-time-step Adams–Bashforth scheme with a fixed error tolerance. To describe the motion of the vortex sheet, we follow markers that travel along the sheet with a speed that is the average of the fluid speed on either side of the sheet, whereas Rottman *et al.* followed markers that travel with the speed of the fluid just inside the

sheet. The important distinction between these two approaches is that the vorticity strength of the markers is independent of time in the present formulation and time dependent in the other (and therefore an additional equation must be solved to determine this time dependence).

The results of our present attempt to determine the critical time are summarized in table 1. Calculations were performed for six values of $N = 2^m, m = 4, 5, \ldots, 9$, using double-precision arithmetic on a Silicon Graphics Iris 4D/340VGX workstation (about 16 decimal digits) with $\epsilon = 10^{-13}$ and $\Delta t = 10^{-3}$. We monitored two measures of the critical time: the first, t_f^N (also used by Rottman *et al.*), is the time when all the Fourier amplitudes of z first become greater than ϵ (and therefore the filter is no longer effective) and the second, t_s^N (also used by Krasny 1986*a*), is the time at which a minimum separation $S_{\min}^N$ between any pair of points is attained. As shown in table 1, t_f^N increases and t_s^N decreases as N increases. Assuming that both these times have the behaviour $a_0 + a_1 N^{-1}$ for large N, we extrapolated them to $N = \infty$ using a least-squares fit to the values for $N = 128$, 256 and 512. These extrapolated results are shown on the last line of table 1. Apparently $t_f^\infty = 0.60$ and $t_s^\infty = 0.59$. It can be argued that t_f^∞ should occur just after t_c as Pugh (1989) noted, so we choose $t_c = t_s^\infty = 0.59$ as our estimate of the critical time. Also shown in table 1 is the value of $S_{\min}^N$ and its value extrapolated to $N = \infty$. This extrapolated value should be zero and the non-zero value shown in the table is an indication of the error involved in these extrapolations.

In table 2 we list the radius of curvature R and the Lagrangian parameter ξ_c (where $\xi = \pm\xi_c$ are the locations on the sheet) for the points where R is a minimum $R_{\min}$ at the critical time $t_c = 0.59$, for the six values of N. The magnitude of R decreases as N increases implying that the curvature is infinite at t_c. Interestingly the curvature changes sign for $R = R_{\min}$ with $N = 128$ and 256. Another estimate of t_c is to determine the time when the curvature first changes sign. We have done this and using the same procedure as before we extrapolated to $N = \infty$ and obtained the same result $t_c = 0.59$. The value of ξ_c apparently oscillates as a function of N about the value of $\xi_c \approx 0.80$ ($\approx \frac{1}{4}\pi$).

Also listed in table 2 are the position X on the x-axis of the vortex sheet's centroid and the fractional increase of the arclength $S' = (S - 2\pi)/2\pi$, where S is the arclength of the sheet computed by summing the distances between consecutive pairs of points, at $t = 0.59$ for the six values of N. Note that the centroid position converges very rapidly and that arclength appears to converge to a finite value at the critical time.

The estimate of the critical time $t_c \approx 0.59$ obtained here is different from $t_c \approx 0.55$ obtained by Rottman *et al.* (1987). The difference is most likely attributable to the errors associated with the filtering procedure in combination with a different time integration scheme. In particular, the variable step length method used by Rottman *et al.* makes the error associated with the filtering difficult to assess. Probably, the variable step method took larger time steps, so the filter was applied less often allowing spurious errors to grow more rapidly than in the present case. On the other hand, we may be applying the filter too often so that the time growth of the high-wavenumber components is suppressed.

Now that we have an estimate of the critical time using the Runge–Kutta integration scheme, we wish to explore more carefully the nature of the singularity that forms at $t = t_c$ at the points $\xi = \pm\xi_c$. We follow the methods introduced by Sulem, Sulem & Frisch (1983) in which the singularity in the vortex sheet is assumed to occur when a branch point in the complex plane, which has a position that is a function of time, reaches the real axis. Specifically, consider a complex function

N	t_f^N	t_s^N	$S_{\min}^N$
16	0.037	0.714	0.1600
32	0.208	0.662	0.0597
64	0.380	0.626	0.0262
128	0.491	0.607	0.0124
256	0.548	0.597	0.0061
512	0.574	0.595	0.0037
⋮	⋮	⋮	⋮
∞	0.60	0.50	0.001

TABLE 1. Estimation of the critical time as a function of N: t_f^N is the time when the Fourier filter is no longer effective with a threshold of 10^{-13}, t_s^N is the time of minimum separation of any adjacent pair of vortices, and $S_{\min}^N$ is the minimum separation of any adjacent pair of vortices. The values corresponding to $N = \infty$ were obtained by linear extrapolation for the three largest values of N.

N	ξ_c	$R_{\min}$	$\Gamma_{\max}$	X	$1/S'$
16	0.982	0.332	2.712	0.03769	26.45
32	0.884	0.275	2.797	0.03771	26.54
64	0.834	0.210	2.893	0.03771	26.52
128	0.761	0.117	3.024	0.03771	26.50
256	0.773	0.037	3.273	0.03771	26.48
512	0.804	0.015	3.951	0.03771	26.38

TABLE 2. Properties of the vortex sheet as a function of N at $t = 0.59$. ξ_c is the Lagrangian position of the maximum of the absolute value of the curvature, $R_{\min}$ is the inverse of the absolute value of the curvature at ξ_c, $\Gamma_{\max}$ is the value of Γ at ξ_c, X is the centroid position and S' is the fractional increase of the arclength of the sheet.

$z(\xi, t) = x(\xi, t) + iy(\xi, t)$ that at any specified time is a function of the real variable ξ. To match the periodic and symmetry properties of the vortex sheet of interest here, we require $z(\xi, t)$ to satisfy the constraint

$$z^*(\xi \pm n2\pi, t) = z(-\xi \pm n2\pi, t) \quad \text{for} \quad n = 0, 1, 2, \ldots, \text{ and } -\pi \leqslant \xi \leqslant \pi. \tag{3.1}$$

We assume that $z(\xi, t)$ can be continued onto the complex plane $\zeta = \xi + i\eta$ and furthermore that z has branch points at $\zeta_{+n} = \zeta_0 \pm n2\pi$ in the neighbourhood of which z behaves as

$$z = C(\zeta - \zeta_{+n})^{\mu}, \tag{3.2}$$

where in general C and μ are complex. It follows from (3.1) that another set of branch points must exist at $\zeta_{-n} = -\zeta_0^* \pm n2\pi$ where z behaves as

$$z = C^* e^{i\mu^*\pi}(\zeta - \zeta_{-n})^{\mu^*}, \tag{3.3}$$

in which a superscript asterisk denotes a complex conjugate. All C, μ and ζ_0 are functions of time. The idea is that, as time increases, the branch points trace a path in the complex plane that reaches the real axis ($\eta_0 = 0$) at $t = t_c$, and $C(t_c)$ and especially $\mu(t_c)$ describe the nature of the singularity that appears spontaneously at two points on the vortex sheet at t_c.

We can obtain estimates of C, μ and ζ_0 by computing the Fourier coefficients of z. Since $z(\xi, t)$ is periodic with period 2π, it can be represented as a Fourier series

$$z(\xi, t) = \sum_{k=-\infty}^{\infty} \hat{z}_k(t) \exp(-ik\xi) \tag{3.4}$$

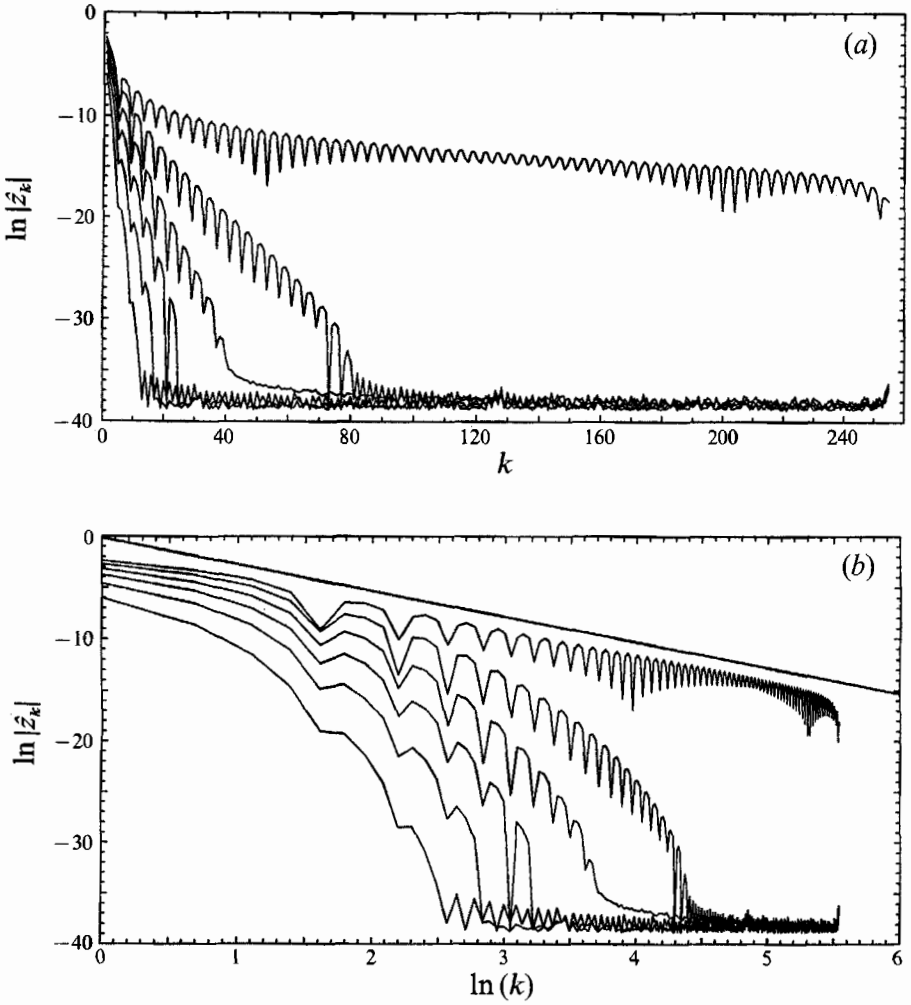

FIGURE 2. Plots of the magnitudes of the Fourier coefficients $|\hat{z}_k|$ for the vortex sheet position as a function of the positive wavenumber k at $t = 0.1$, 0.2, 0.3, 0.4, 0.5 and 0.585: (*a*) $\ln|\hat{z}_k|$ versus k, and (*b*) $\ln|\hat{z}_k|$ versus $\ln|k|$. The $\hat{z}_k$ were computed from the calculations with $N = 512$. The straight line in (*b*) has slope -2.5.

where the Fourier coefficients are given by

$$\hat{z}_k(t) = \frac{1}{2\pi}\int_{-\pi}^{\pi} z(\xi, t)\exp(\mathrm{i}k\xi)\,\mathrm{d}\xi. \tag{3.5}$$

Using an asymptotic analysis analogous to that outlined by Carrier, Krook & Pearson (1966, p. 255), we can show that

$$\hat{z}_k \sim A|k|^{-\mathrm{Re}(\mu)-1}\,\mathrm{e}^{-k\eta_0}\sin[k\xi_0 - \mathrm{Im}(\mu)\ln|k| + \phi] \tag{3.6}$$

for large $|k|$, in which A and ϕ are real and $\mathrm{Re}(\mu)$ and $\mathrm{Im}(\mu)$ denote the real and imaginary parts, respectively, of μ. The contributions to $\hat{z}_k$ are due entirely to the two branch points at $\zeta = \zeta_0$ and $\zeta = -\zeta_0^*$, through the use of Cauchy's theorem and Jordan's Lemma, and the large-$|k|$ asymptotic behaviour is obtained using Laplace's method. Note that $\eta_0(t)$ is positive when k is positive and negative when k is negative and that A, μ, ζ_0 and ϕ can be different for negative and positive k.

	$2 \leqslant k \leqslant 240$		$6 \leqslant k \leqslant 240$	
t	η_0	Re (μ)	η_0	Re (μ)
0.300	0.736	2.348	0.523	5.162
0.350	0.599	2.207	0.481	4.019
0.400	0.458	2.181	0.399	3.335
0.450	0.322	2.156	0.300	2.725
0.500	0.207	1.997	0.209	2.030
0.550	0.090	1.773	0.096	1.544
0.585	−0.001	1.596	0.003	1.313

TABLE 3. Linear least-squares estimates of $\eta_0(t)$ and Re $[\mu(t)]$ for $0.300 \leqslant t \leqslant 0.585$ based on the $N = 512$ calculation shown in figure 2 for two ranges of wavenumbers (excluding all $|\hat{z}_k| \leqslant \epsilon$)

From (3.6) we see that when $t < t_c$ the Fourier coefficients decay exponentially with k, which means $z(\xi, t)$ is analytic. But at $t = t_c$, when $\eta_0 = 0$, the Fourier coefficients decay algebraically with k and the decay rate Re $(\mu)+1$ describes the nature of the irregularity of $z(\xi, t_c)$ at $\xi = \xi_0$. We can obtain qualitative estimates of $\mu(t)$ and $\eta_0(t)$ by computing $\hat{z}_k(t)$ using fast Fourier transforms with $-\frac{1}{2}N \leqslant k \leqslant \frac{1}{2}N$ and comparing the computed $\ln|\hat{z}_k|$ with the expression (from 3.6)

$$\ln|\hat{z}_k| \sim \ln|A| - [\mathrm{Re}\,(\mu)+1]\ln|k| - \eta_0|k| + \ln|\sin[k\xi_0 - \mathrm{Im}\,(\mu)\ln|k| + \phi]|. \quad (3.7)$$

Figure 2(*a*) is a plot of $\ln|\hat{z}_k|$ versus positive k for $0.100 \leqslant t \leqslant 0.585$ for the case with $N = 512$. The oscillatory character of these curves is due to the last term in (3.7). Sulem *et al.* (1983) remarked that if several singularities are relevant asymptotically for large $|k|$ then $|\hat{z}_k|$ may exhibit an oscillatory behaviour. Ignoring the superimposed oscillation for now, the curves clearly have a linear behaviour for large $|k|$ for all t except $t = 0.585$. This behaviour indicates that the exponential term in (3.6) is dominant for these early times. At $t = 0.585$ the curve has a logarithmic character. This logarithmic character can be seen more clearly in figure 2(*b*) in which $\ln|\hat{z}_k|$ versus $\ln|k|$ is plotted so that a logarithmic curve appears as a straight line. Thus, near the critical time, η_0 is small and the spectrum is dominated by the algebraic term in (3.6). The slope of this straight line gives an estimate of Re $[\mu(t_c)+1]$. Moore (1979) using an approximate analytical theory found that Re $[\mu(t_c)+1] = 2.5$ for the singularity that forms on an initially flat vortex sheet and Pugh (1989) estimated that this is also true for a buoyant circular vortex sheet. We have plotted a straight line with slope -2.5 in figure 2(*b*); it compares well at least in a qualitative sense with the algebraic decay of the computed Fourier coefficients at $t = 0.585$.

In summary, figures 2(*a*) and 2(*b*) show that $\eta_0(t)$ decreases monotonically to near zero as $t \to t_c$ and at least qualitatively Re $[\mu(t_c)+1] \approx 2.5$. To obtain more quantitative estimates of $\mu(t)$ and $\eta_0(t)$ we used a least-squares method to fit the first three terms in (3.7) to the curves plotted in figure 2. The results for $\eta_0(t)$ and Re $[\mu(t)]$ are listed in table 3 for two ranges of wavenumbers: $2 \leqslant k \leqslant 240$ and $6 \leqslant k \leqslant 240$ (excluding all $|\hat{z}_k| < \epsilon$). The estimates of $\eta_0(t)$ are fairly consistent for the two ranges of wavenumbers and show that $\eta_0(t)$ does indeed decrease monotonically with increasing t, as expected. We have plotted these values of $\eta_0(t)$ versus t in figure 3 and it is clear that $\eta_0(t)$ decreases linearly with increasing t. The estimates for Re (μ) are not as consistent, but for $t \approx t_c$ seem to stay in the range $1.3 <$ Re $(\mu) < 1.6$. Similar results were found for negative k.

As noted by Sulem *et al.* (1983), it is difficult to compute $\eta_0(t_c)$ accurately using a

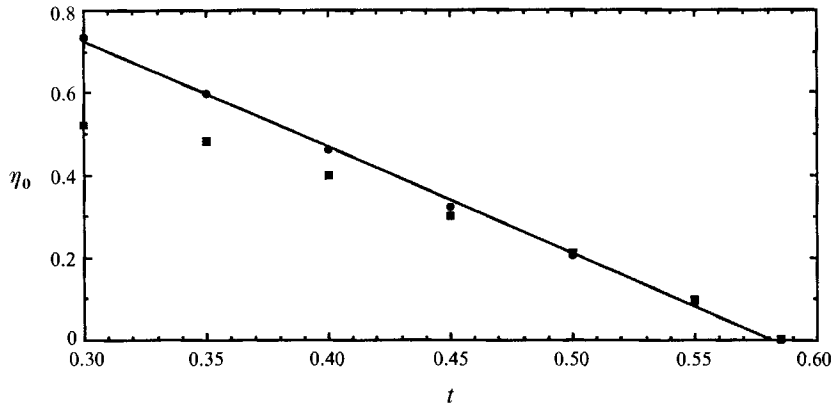

FIGURE 3. The logarithmic decrement $\eta_0(t)$ as a function of time for the calculation with $N = 512$, as listed in table 3: •, η_0 estimated for $2 \leqslant k \leqslant 240$; ▪, η_0 estimated for $6 \leqslant k \leqslant 240$. The straight line is a least-squares fit to the data points for $2 \leqslant k \leqslant 240$.

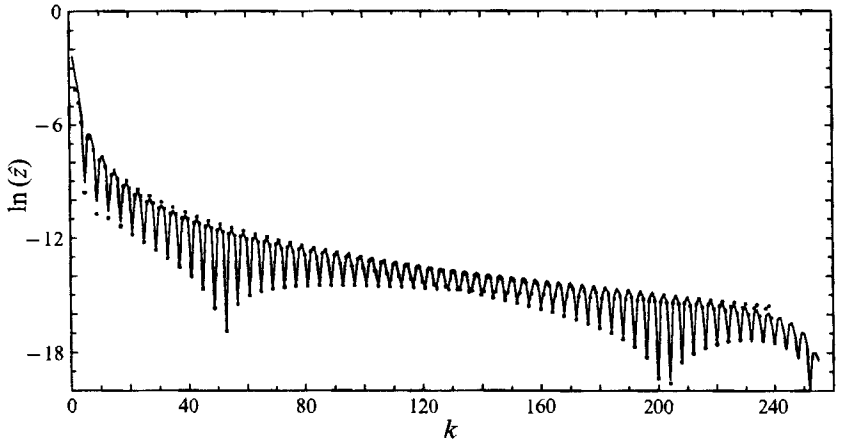

FIGURE 4. A comparison of the magnitudes of the Fourier coefficients $|\hat{z}_k|$ for the vortex-sheet position with the asymptotic formula (3.7): ——, computed $\ln|\hat{z}_k|$ for positive k with $N = 512$ at $t = 0.585$; •, from (3.7) with $A = 0.09$, $\mathrm{Re}\,(\mu) = 1.20$, $\mathrm{Im}\,(\mu) = 0.14$, $\eta_0 = 0.005$, $\xi_0 = 0.79$, $\phi = 2.58$; these coefficients were computed using the Levenberg–Marguardt nonlinear least-squares method to fit (3.6) to the computed values of $\hat{z}_k$ for positive wavenumbers k in the range $2 \leqslant k \leqslant 240$.

truncated Fourier series. This is because the truncation error becomes significant when $1/\eta_0 \gtrsim \frac{1}{2}N$. Therefore, the Fourier series representation of $z(\xi, t)$ becomes inaccurate when η_0 is less than or comparable to the spatial mesh size. We have chosen $t_c \approx 0.585$ for figures 2 and 3 because this is the time at which $\eta_0 \approx 2/N$ when $N = 512$.

We have not made an extensive effort to compare all the terms in (3.7) with the curves in figure 2. However, as an example of the type of fit that can be achieved using the full expression, in figure 4 we have plotted (3.7), with the values of A, μ, ξ_0, η_0 and ϕ computed using the Levenberg–Marguardt method to obtain a nonlinear least-squares fit, along with the computed values of $\ln|\hat{z}_k|$ (with k positive) for $t = 0.585$. The agreement is very good for large k except for k near $\frac{1}{2}N$, where of course truncation errors are significant in the computed values for $\hat{z}_k$. The results for negative k (not shown) are similar. The fit is not nearly as good if it is assumed that $\mathrm{Im}\,(\mu) = 0$, and we acknowledge Pugh (1989) for the idea of allowing μ to be complex.

Note in particular that the nonlinear least-squares method gives $\xi_0 = 0.79$ at $t = 0.585$, very close to $\xi_c = 0.80$ as shown in table 2 for $t = 0.59$. This result implies that indeed $\lim_{t \to t_c} \xi_0(t) = \xi_c$, as presumed.

The results of this section provide some useful guidelines for exploring the behaviour of the δ-equations. Krasny's (1986*b*) assumption about the regularity of the solutions of the δ-equations can be interpreted as an assumption that $\eta_0(t)$ is bounded away from zero for all t or at least $\eta_0(t) \to 0$ only as $t \to \infty$ when $\delta^2 > 0$. Therefore, an inspection of the Fourier coefficients as a function of k for different times should give an indication of how $\eta_0(t)$ behaves for the δ equations and therefore if Krasny's assumption is correct. For example, if $\eta_0(t)$ decays linearly with time, then we know that at some finite time the vortex sheet will develop a singularity, and therefore Krasny's assumption is incorrect. On the other hand, if $\eta_0(t)$ is found to decay exponentially with time, then $\eta_0(t) \to 0$ only as $t \to \infty$ and Krasny's assumption is valid.

4. Numerical results with $\delta^2 > 0$

In this section we summarize the results for the problem formulated in §2 with $\delta^2 > 0$, and compare the limit of these results as $\delta^2 \to 0$ with the results of the previous section.

The calculations described in this section were performed on the Amdahl VP1100 at the Manchester Computer Centre using double-precision arithmetic (approximately 16 decimal digits). The operations necessary to evaluate (2.4) were vectorized so that they could be executed at far greater speed than if they were performed sequentially.

4.1. *General properties of the small-time solution*

Figure 5(*a*) shows the evolution of the vortex sheet up to $t = 4.0$, as computed by the vortex-blob method using $\delta = 0.1$, $N = 625$, and $\Delta t = 0.01$. For these values of δ and t the solution shown in figure 5 would be unchanged within the plotting accuracy by any refinement of the mesh parameters N and Δt. The vortex sheet initially deforms into a horseshoe-like shape with the open end of the shoe pointing downstream and the centre of mass of the released fluid accelerates in the downstream direction. Some time between $t = 1.0$ and 2.0 the open end of the horseshoe begins to roll up into two spirals as the centre of mass continues to accelerate. For $t > 2.0$ the outer shape of the vortex sheet changes very little, but the number of turns in the inner spirals increases as time progresses and become more closely spaced. At $t = 3.0$ the acceleration of the centre of mass is reduced significantly and the vortex sheet is nearly a distributed vortex pair propagating downstream at a nearly constant speed slightly less than U_0.

Figure 5(*b*) shows a similar calculation except with $\delta = 0.05$. Again, N and Δt were small enough so that the solution is converged to within plotting accuracy. The outer shape of the evolving vortex sheet is only slightly different than that shown in figure 5(*a*), but the details of the inner spirals are significantly different. With the smaller value of δ, the spirals begin to form before $t = 1.0$ and at later times have more turns than the $\delta = 0.1$ case. The acceleration of the centre of mass is nearly the same for the two cases. In general, the gross features of the evolution of the vortex sheet are fairly insensitive to the value δ; only the detailed structure of the inner core of the spirals changes significantly as δ is reduced. N must be increased as δ is decreased in order to fully resolve the inner structure of the spirals.

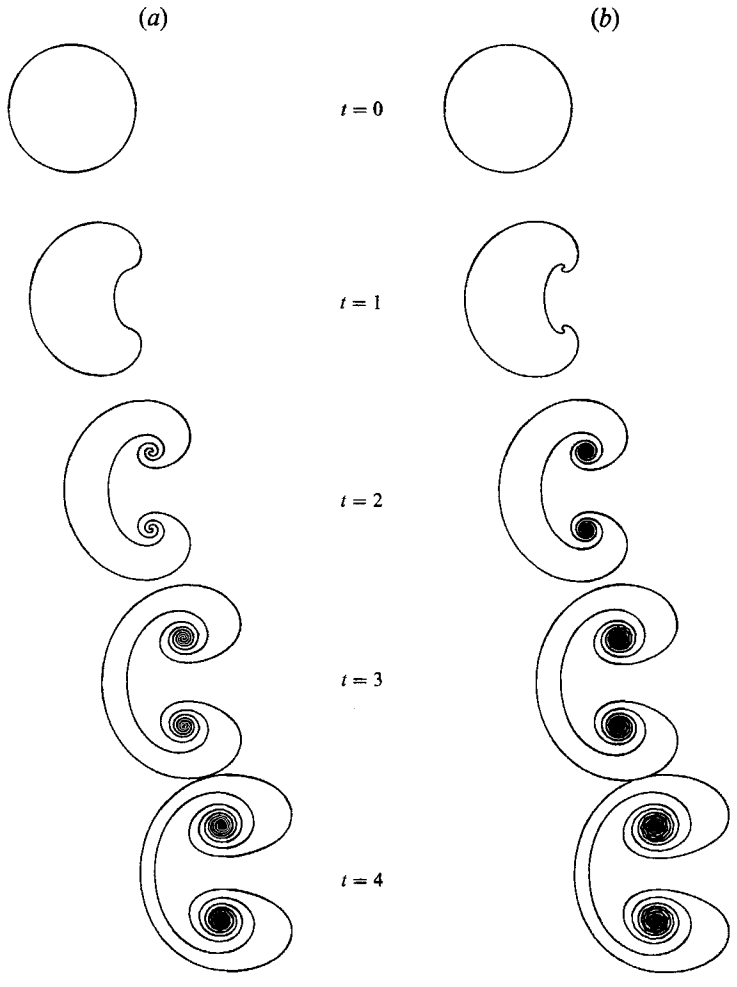

FIGURE 5. Numerical solutions of the δ-equations at $t = 0$, 1, 2, 3, and 4, computed with $N = 625$, $\Delta t = 0.01$ and $\epsilon = 0$: (*a*) $\delta = 0.1$, (*b*) $\delta = 0.05$.

As an example of how the solution converges as $N \to \infty$, figure 6 shows a close-up plot of one of the spirals at $t = 1.0$ using $N = 625$, 1250, and 2500 points with $\delta = 0.02$. With $N = 625$ the inner turns of the spiral are overlapping, but outside the innermost turns the plot is identical to those with $N = 1250$ and 2500. All regions of the plots are identical with $N = 1250$ and 2500, showing that convergence within plotting accuracy has been achieved with $N = 1250$.

For all the calculations we have presented, the time step was chosen such that the Hamiltonian function was preserved to within at least four significant digits and to within six significant digits for $t < t_c$. With $\delta = 0.02$ the sheet became unstable at some time between 1.0 and 2.0 and it was necessary to use the spectral filter to prevent this. Otherwise, for the calculations presented in this section the value of δ was large enough to prevent spurious perturbations from destabilizing the calculations for these short time periods ($t \leqslant 4.0$). In all subsequent calculations with $\delta \leqslant 0.02$, the spectral filter was used to prevent the appearance of irregular motion due to round-off error.

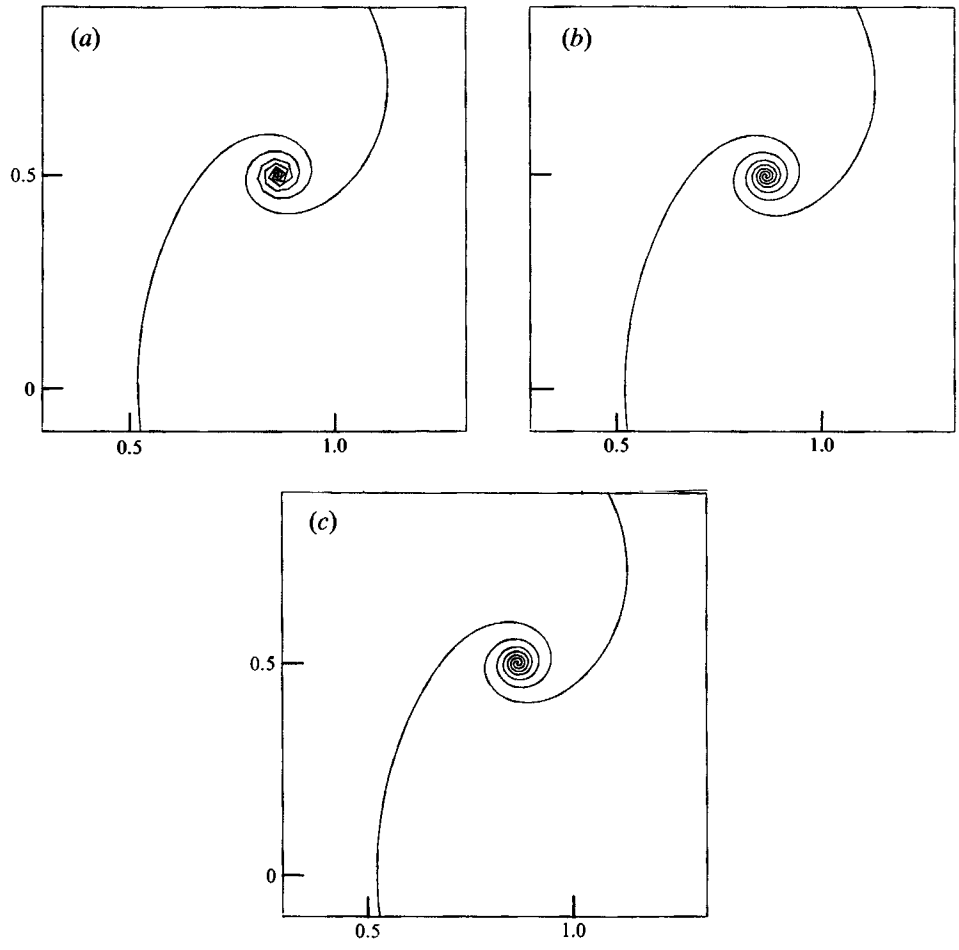

FIGURE 6. An enlarged view of one of the spirals at $t = 1.0$, computed using the δ-equations with $\delta = 0.02$ and $\epsilon = 0$: (*a*) $N = 625$, (*b*) $N = 1250$, and (*c*) $N = 2500$.

δ		X	$1/S'$	$R_{\min}$
0.2515		0.11691	477.1	0.84405
0.1005		0.06091	137.9	0.71892
0.0503		0.04162	95.69	0.64928
0.0201		0.03005	69.67	0.59306
0.01005		0.02619	63.71	0.57022
0.00503		0.02431	60.90	0.55768
0	(i)	0.0224	58.1	0.545
	(ii)	0.0223	62.0	0.550
	(iii)	0.0224	58.2	0.544

TABLE 4. The computed values of the centroid position X, the inverse fractional increase of the arclength $1/S'$, and the minimum radius of curvature $R_{\min}$ as functions of δ at $t = 0.5$. The values for $\delta = 0$ were obtained from: (i) linear extrapolation using values for $\delta = 0.005$ and 0.01; (ii) extrapolation using the least-squares, quadratic polynomial approximation for all δ-values; (iii) the vortex-sheet calculation by Rottman *et al.* (1987), as indicated

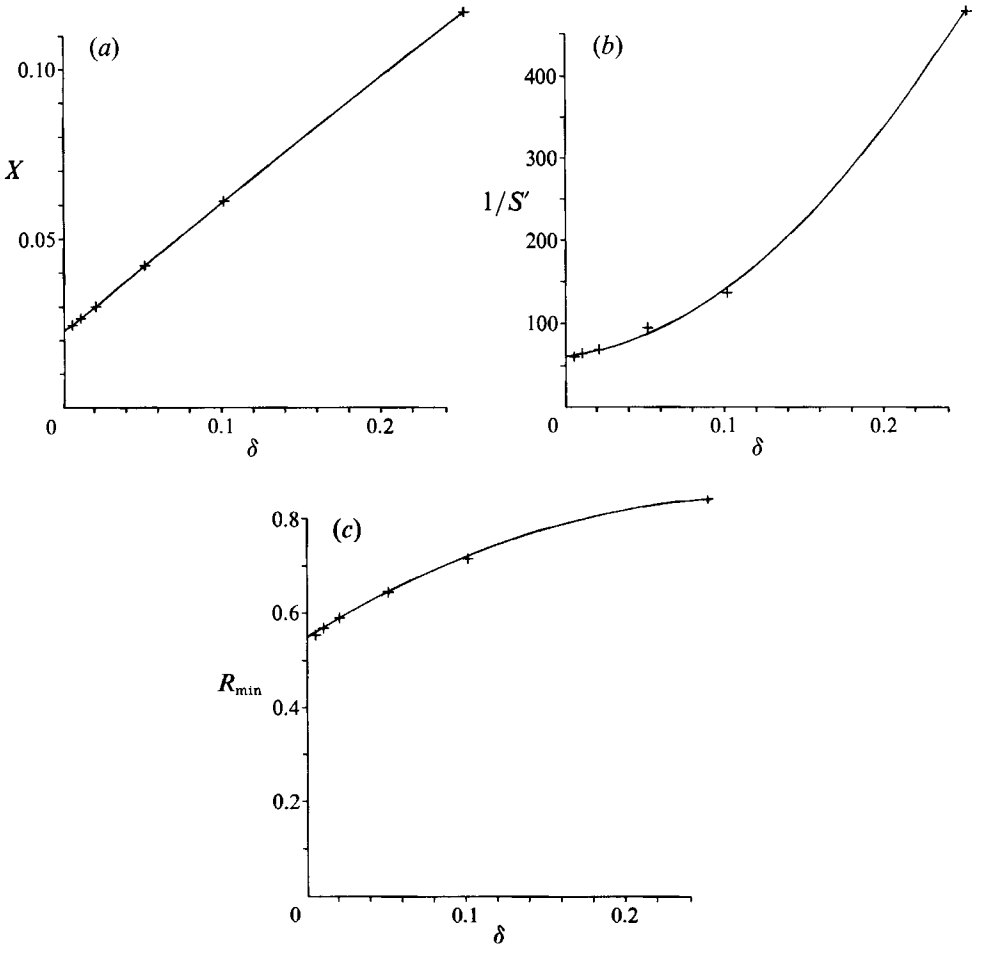

FIGURE 7. Features of the solutions of the δ-equations as functions of δ at $t = 0.5$. The points are the converged computed values and the solid curve is a quadratic polynomial fitted to the points using a least-squares criterion: (*a*) the centroid positions X, (*b*) the inverse fractional increase in the arclengths $1/S'$, and (*c*) the minimum radius of curvature $R_{\min}$.

4.2. *Convergence as* $\delta^2 \to 0$ *when* $t < t_c$

For times before the critical time t_c, we were able to compute the centre-of-mass position X, the fractional increase of the arclength S', and the minimum radius of curvature $R_{\min}$ to an accuracy of at least four significant figures for values of the smoothing parameter in the range $0.005 \leqslant \delta \leqslant 0.25$. The values we obtained for these quantities are listed in table 4 and plotted in figure 7 for $t = 0.5$ as a function of δ. The solid lines in figure 7 were obtained by using a least-squares approximation to fit a quadratic polynomial to the data values. The good fit of these curves with the data indicates that in the limit as $\delta \to 0$ these quantities behave as an asymptotic power series in δ; for example,

$$X(\delta, t) = X(0, t) + c_1 \delta + c_2 \delta^2 + \ldots, \tag{4.1}$$

where $c_1, c_2, \ldots$ are functions of time only. The extrapolated values corresponding to $\delta = 0$ are listed in table 4. The values resulting from linear extrapolation using

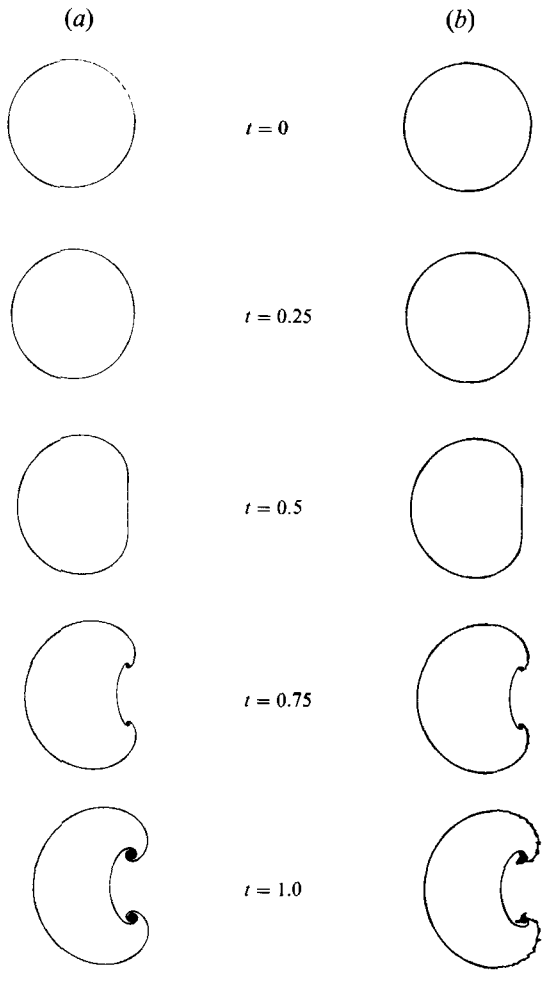

FIGURE 8. Numerical solutions of the δ-equations at $t = 0$, 0.25, 0.50, 0.75 and 1.0 computed with $\delta = 0.01$, $N = 1250$, $\Delta t = 0.01$; (*a*) $\epsilon = 2.5 \times 10^{-15}$, and (*b*) $\epsilon = 2.5 \times 10^{-16}$.

$\delta = 0.005$ and 0.01 are also listed along with the values from the vortex-sheet calculation. All these values are converged to the number of figures displayed. The values obtained from the linear extrapolation are in very close agreement with the vortex-sheet values and those obtained from the quadratic polynomial least-squares approximation are in less close agreement. From these results, we conclude that the solution of the δ equations converges to the exact solution in the limit $\delta \to 0$, when $t < t_c$.

4.3. *Irregular motion when* $t > t_c$

Figure 8 shows the evolution of our vortex sheet with $\delta = 0.01$ and $N = 1250$ for times up to $t = 1.0$. In figure 8(*a*) the filter parameter ϵ was set to 2.5×10^{-15}, and the solution is seen to be stable at $t = 1.0$. In figure 8(*b*), ϵ was reduced to 2.5×10^{-16}, which is very close to the machine precision of 2.2×10^{-16}, and irregular motion is evident at $t = 0.75$ and has grown substantially by $t = 1.0$. With $\delta = 0.02$ the spectral filter with $\epsilon = 2.5 \times 10^{-15}$ produced stable solutions up to $t = 4.0$ (the maximum time investigated).

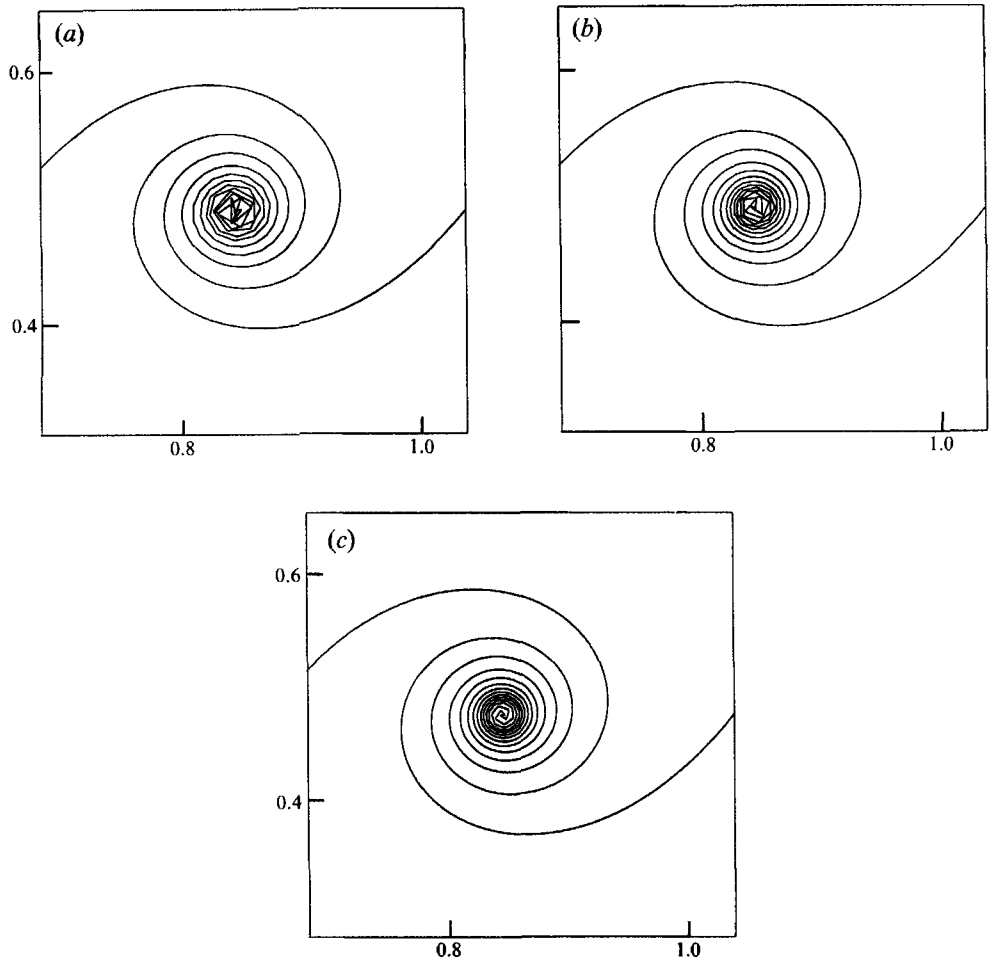

FIGURE 9. An enlarged view of one of the spirals at $t = 1.0$ computed with $\delta = 0.01$ and $\epsilon = 10^{-16}\,(\frac{1}{2}N)^{\frac{1}{2}}$: (*a*) $N = 2500$, (*b*) $N = 5000$, and (*c*) $N = 10000$.

Evidence that the solution converges with $\delta = 0.01$ at $t = 1.0$ with $\epsilon = 10^{-16}\,(\frac{1}{2}N)^{\frac{1}{2}}$ is presented in figure 9. This figure shows close-up plots of the spiral at $t = 1.0$ computed using $N = 2500$, 5000 and 10000. With $N = 2500$ and 5000 the innermost turns of the spiral overlap but the outer turns are well resolved and the amount of overlapping decreases as N increases. With $N = 10000$ the entire spiral is well resolved. (The calculation with $N = 10000$ required 90 minutes of CPU time.)

In attempting to carry the calculation further in time, we discovered that irregular motion eventually occurs despite the use of the spectral filter. Figure 10 shows close-up plots of one of the spirals at $t = 1.45$, 1.50 and 1.55 for the case with $\delta = 0.01$, $\epsilon = 10^{-16}\,(\frac{1}{2}N)^{\frac{1}{2}}$ and with $N = 5000$ and 10000. At $t = 1.5$ small but definite signs of irregularity appear on the outermost turn of the spiral and these irregularities increase in size and spread over a larger region of the sheet as t increases. Only slight differences are apparent between $N = 5000$ and 10000 at $t = 1.55$.

Although we have not attempted to estimate the precise time t_δ, say, at which the irregular motion first appears as a function of δ, our calculations indicate that $t_\delta \to t_c$ as $\delta \to 0$. Figure 11 shows plots of the spirals for $\delta = 0.005$, $\epsilon = 10^{-16}\,(\frac{1}{2}N)^{\frac{1}{2}}$ and

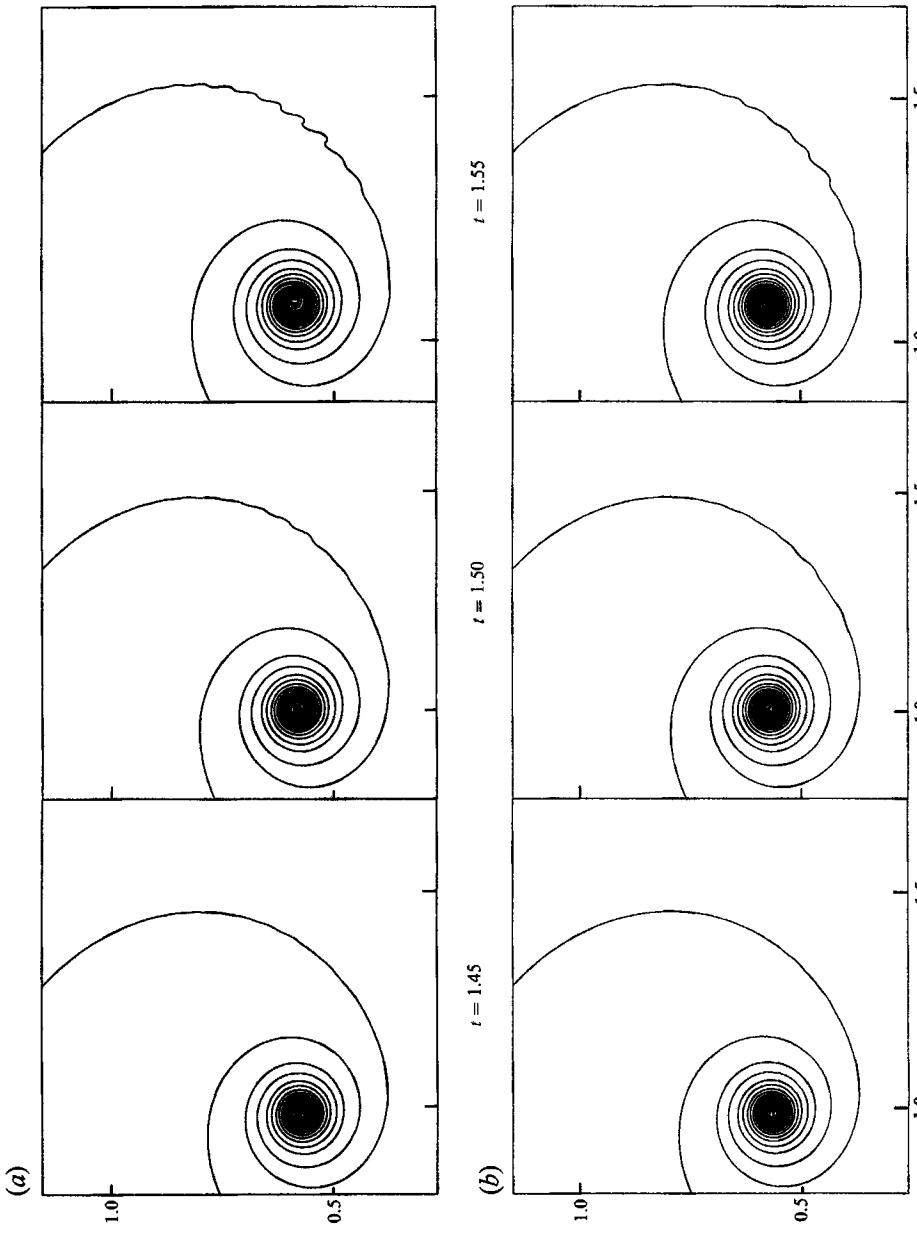

FIGURE 10. Enlarged views of one of the spirals with $\delta = 0.01$ and $\epsilon = 10^{-16}$ $(\frac{1}{2}N)^{\frac{1}{2}}$ at $t = 1.45$, 1.50 and 1.55 showing the onset of irregular motion: (*a*) $N = 5000$; (*b*) $N = 10000$.

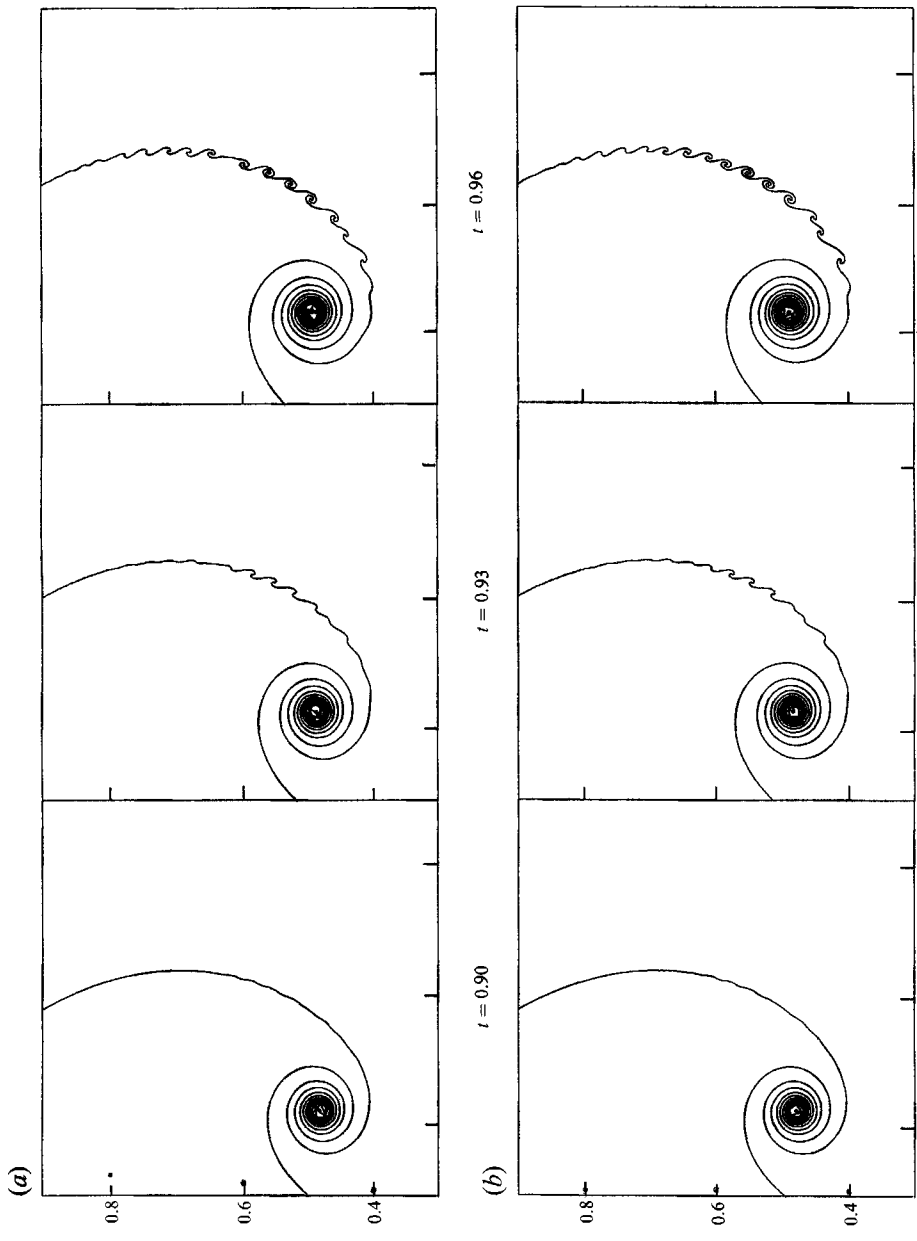

FIGURE 11. Enlarged views of one of the spirals with $\delta = 0.005$ and $\epsilon = 10^{-16}$ $(\frac{1}{2}N)^{\frac{1}{2}}$ at $t = 0.90$, 0.93 and 0.96 showing the onset of irregular motion: (*a*) $N = 5000$; (*b*) $N = 10000$.

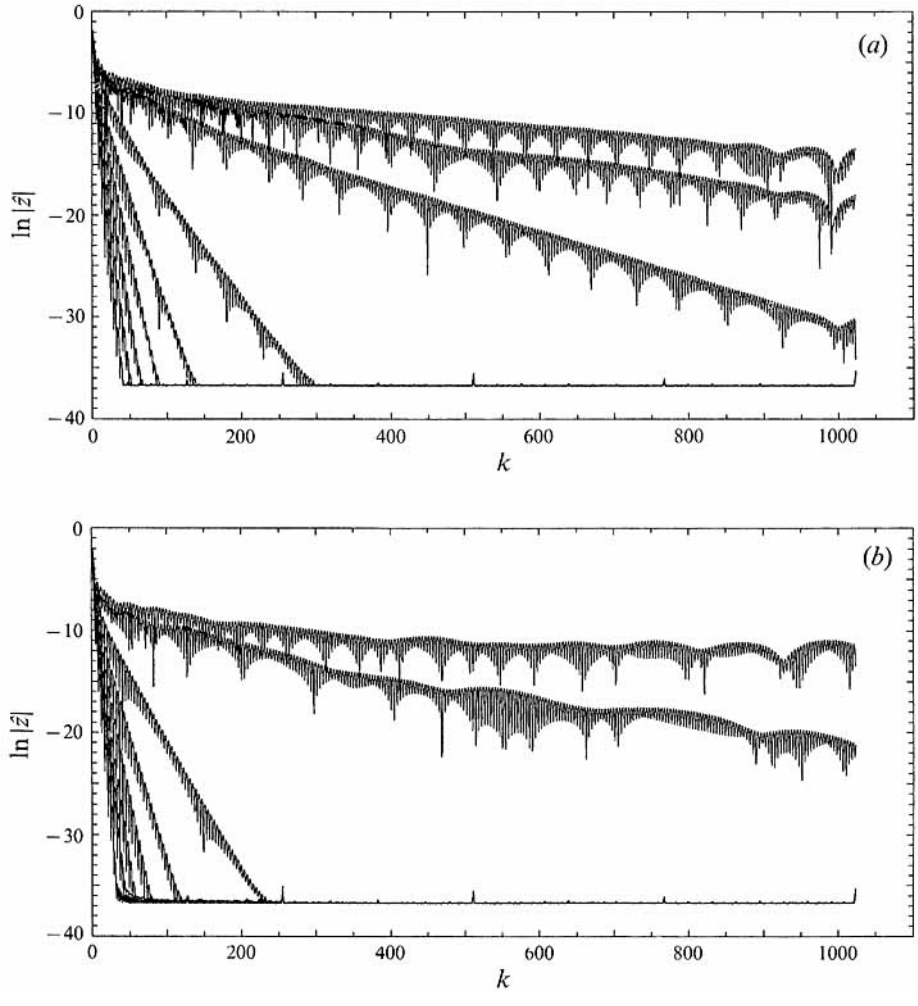

FIGURE 12. Log-linear plots of the Fourier coefficient amplitudes versus wavenumber (for positive wavenumbers) with $N = 2048$, $\epsilon = 3.2 \times 10^{-15}$ and (*a*) $\delta = 0.01$ for $t = 0.4, 0.45, \ldots, 0.8$; (*b*) $\delta = 0.005$, for $t = 0.4, 0.45, \ldots, 0.7$.

with $N = 5000$ and 10000 at $t = 0.90$, 0.93 and 0.96. Irregular motion is clearly developing at an earlier time than with $\delta = 0.01$ and there is no apparent difference between $N = 5000$ and 10000. (With $\delta = 0.02$ such irregular motion had not developed at $t = 4.0$.)

The behaviour of the discrete Fourier transforms of the solutions could give some insight into the origin of the irregular motion. The computed Fourier coefficients of the solutions for the complex positions $z = x + iy$ of the points on the sheet with $\delta = 0.005$ and 0.01 are plotted in figure 12 as functions of the positive wavenumber k for successive times. At early times the logarithm of the Fourier coefficients' amplitudes decrease rapidly as k increases until the level of machine precision is reached. Without the superimposed small-scale oscillations the decay would be almost linear. As time increases the slope of this linear curve increases and the rate of increase is related inversely to the magnitude of δ so that at some time after t_c the spectrum rapidly changes from linearly decreasing to apparently logarithmically decreasing (which indicates that the vortex sheet has become non-analytic) and

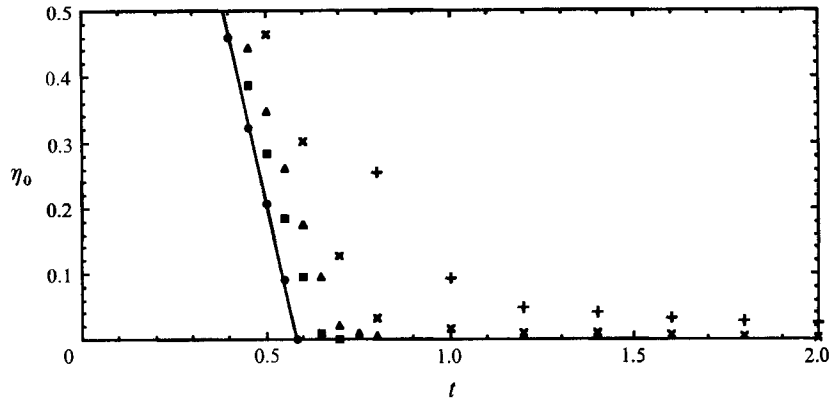

FIGURE 13. The logarithmic decrement $\eta_0(t)$ computed from a linear least-squares fit to the logarithm of Fourier coefficients for positive wavenumbers: •, $\delta = 0$, $N = 512$, $2 \leqslant k \leqslant 240$; ▪, $\delta = 0.005$, $N = 2048$, $2 \leqslant k \leqslant 1000$; ▲, $\delta = 0.01$, $N = 2048$, $2 \leqslant k \leqslant 1000$; ×, $\delta = 0.02$, $N = 2048$, $2 \leqslant k \leqslant 1000$; +, $\delta = 0.05$, $N = 1024$, $2 \leqslant k \leqslant 500$. The straight line is a least squares fit to $\eta_0(t)$ for $\delta = 0$, taken from figure 3.

eventually develops a larger-scale superimposed wavy appearance for large k. This occurs well before t_δ; for example with $\delta = 0.01$ it is just evident at $t = 0.8$ whereas $t_\delta \approx 1.5$ for this case. At t_δ (not shown here) the large-scale waviness appears over the entire range of wavenumbers. This type of spectral evolution is similar to that for $\delta = 0$ as $t \to t_c$ as described in §3; in other words the irregular motion could be a result of a spontaneous singularity forming in the exact solution for the vortex sheet.

To obtain a more quantitative description of the time evolution of the Fourier coefficients plotted in figure 12, we used the linear least-squares method described in §3 to estimate the value of $\eta_0(t)$. These estimates, for positive wavenumbers in the range $2 \leqslant k \leqslant 1000$, are plotted in figure 13. Also plotted in this figure for comparison are the linear least-squares estimates of $\eta_0(t)$ for $\delta = 0$, as computed in §3 and shown in figure 3. It appears that η_0 decreases linearly with time for all three values of δ, but the rate of decrease lessens as δ increases. This type of behaviour suggests that a singularity will form in the vortex sheet at some finite time, which appears to be $t = 0.59$, 0.65 and 0.70 for $\delta = 0$, 0.005 and 0.010, respectively. However, this conclusion is tempered by the observation that for the two non-zero values of δ the last one or two data points show evidence of an abrupt change to a much slower rate of decrease. This apparent change in slope occurs at very small values of η_0, so that even with a lessening of the rate of decrease η_0 still approaches zero more rapidly than is possible practically to resolve.

The behaviour of η_0 as it approaches zero is easier to resolve if δ is larger than 0.01. As examples, we have estimated $\eta_0(t)$, again using linear least-squares fits, for two additional cases: $\delta = 0.02$ and 0.05. The results of these calculations are plotted in figure 13. For $\delta = 0.02$, η_0 decreases linearly until about $t = 0.8$ and then changes to a slower clearly asymptotic decrease. For $\delta = 0.05$, η_0 decreases linearly until about $t = 1.0$ and then changes to an even slower rate of decrease. There is no clear indication that a singularity will occur for these two cases.

The totality of these results suggests the following interpretation for the cases with $\delta^2 > 0$. There is an initial rapid linear decrease in η_0 (leading to the initial formation of the spirals) followed by a much slower decrease that asymptotes to zero as $t \to \infty$ (associated with the tightening of the spirals as time increases). For δ^2 not too small,

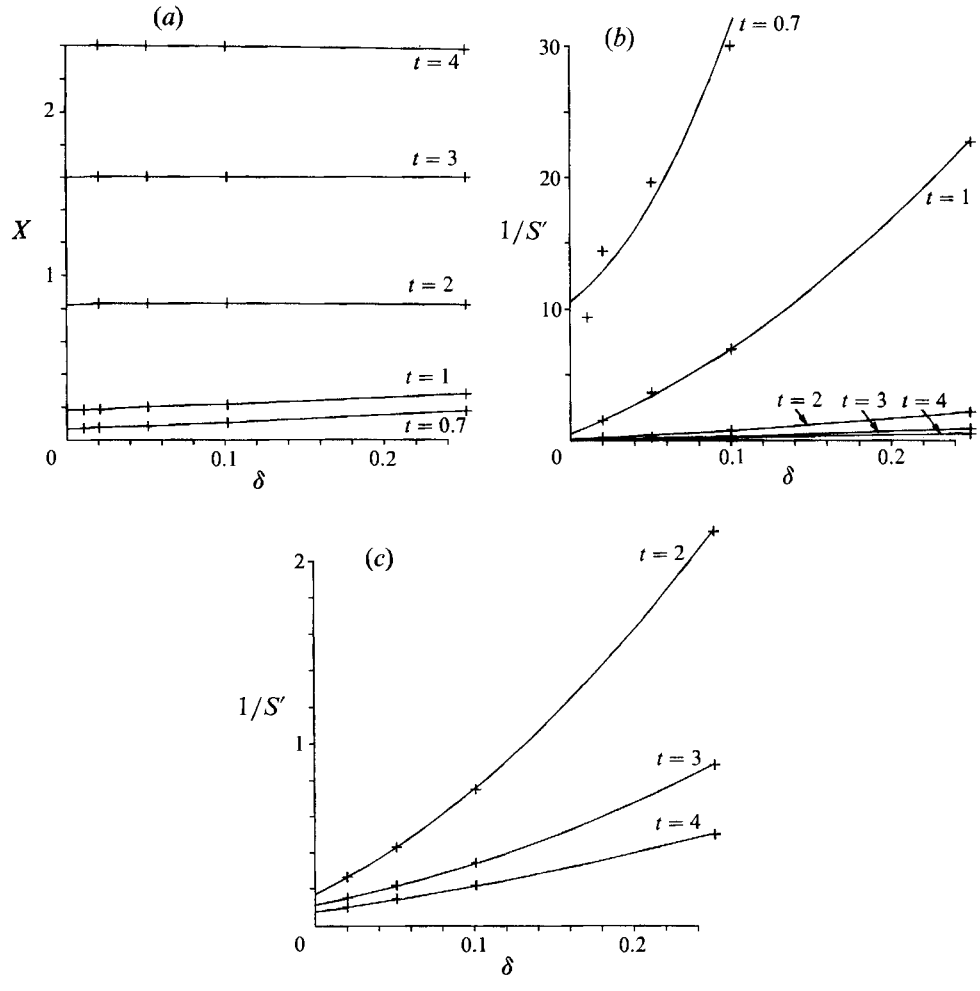

FIGURE 14. Features of the solutions of the δ-equations as functions of δ at $t = 0.7$, 1, 2, 3 and 4. The points are the converged computed values and the solid curves are quadratic polynomials fitted to the points using a least-squares criterion: (*a*) the centroid position X; (*b*) the inverse fractional increase in arclength $1/S'$; (*c*) as (*b*) for $t = 2$, 3, 4 only.

this tightening occurs sufficiently slowly that it is practical in a numerical scheme to increase the resolution appropriately so that the spirals are adequately resolved at some desired time of the evolution of the vortex sheet. For δ^2 very close to zero the spirals tighten so rapidly that for all practical purposes it is impossible to resolve them, leading eventually to aliasing problems that presumably are manifested as the larger-scale irregular motion that we see for $\delta = 0.005$ and 0.01. From a practical point of view, these very small-δ^2 cases behave as if a singularity forms in the sheet at some finite time.

We have performed some sensitivity tests to see if changing ϵ has any effect on the irregular motion for $\delta = 0.005$ and 0.01. These tests indicate that the time of onset of the irregular motion is affected weakly by the choice of ϵ, but otherwise the motion is unchanged.

Also, for $\delta = 0.005$ and 0.01 we experimented with a low-pass digital filter in an attempt to prevent the irregular motion from occurring, based on the hypothesis

that aliasing was causing the problem. The main effect of the filter was to eliminate the fine structure of the spirals. The filter did not prevent the irregular motion. This does not rule out aliasing as the cause of irregular motion but the cause does remain uncertain.

4.4. *The limiting solution as $\delta^2 \to 0$ when $t > t_c$*

The converged values of X and $1/S'$ for several times greater than t_c are plotted as functions of δ in figure 14. We could not obtain accurate results for R_{min} over much of the range of δ shown in the plots when $t > t_c$; apparently the spirals become so tight that the value of R_{min} often becomes less than we can resolve with the number of points that we have used here. We have plotted only the converged values of X and $1/S'$; the values of these quantities did not converge when $t > t_\delta$ (as we have shown) and for $t < t_\delta$ when the inner core of the spiral was not adequately resolved.

Nevertheless, we have fitted quadratic polynomials using the least-squares criterion to the values that did converge as $N \to \infty$ and have extrapolated these curves to $\delta = 0$, as shown in figure 14. The values of X seem to converge as $\delta \to 0$ very well for all the times we have computed, as shown in figure 14(*a*). Indeed, the values seem almost fully converged for $\delta \leqslant 0.25$ with $t \geqslant 2.0$. Similarly the quadratic-polynomial fits to the points for $1/S'$ also appear to converge as $\delta \to 0$ as shown in figures 14(*b*) and14(*c*). Apparently in the limit as $\delta \to 0$, $S' \to \infty$ as $t \to \infty$, indicating that the spirals continue to tighten indefinitely as t increases.

It appears from these results that if moderate values of δ are used for times not greatly larger than t_c, then solutions that converge as $N \to \infty$ can be obtained and these solutions appear to have a limit as $\delta \to 0$.

5. Concluding remarks

We have presented numerical solutions of the δ-equations approximating the two-dimensional inviscid motion of an initially circular vortex sheet released in a cross-flow. When the smoothing parameter $\delta^2 = 0$ (for which the equations are exact), a vortex-sheet method was used to integrate the equations numerically, and when $\delta^2 > 0$ the well-known vortex-blob method was used. For values of δ^2 equal to or close to zero, we used a spectral filter, as recommended by Krasny (1986*a*), to eliminate spurious instabilities due to round-off error.

A detailed study was made of the case with $\delta^2 = 0$. It appears that two singularities form in the vortex sheet at a critical time $t_c \approx 0.59$. The appearance of these singularities is associated with two branch points in the complex plane reaching the real axis at the same time. The presence of two branch points at equal distances from the real axis results in an oscillatory Fourier spectrum of the vortex sheet. Even though the vortex sheet appears only slightly deformed at t_c, analysis indicates that the radius of curvature of the sheet approaches zero as $t \to t_c$ at two points. After t_c the numerical solution did not converge with increasing N.

Our results for $\delta^2 > 0$ indicate that the vortex sheet deforms into two doubly branched spirals. For moderate values of δ^2, and t not too large, these solutions appear to converge with increasing N. However, for very small values of δ^2 the solutions did not converge. We conjectured that the scales associated with these spirals became so small so rapidly that for all practical purposes a singularity had formed in the vortex sheet. Nevertheless, we found that the converged solutions appeared to have a limit as $\delta \to 0$.

It remains unclear what the relation is between the limiting solution as $\delta \to 0$ and the solution with $\delta = 0$ when $t > t_c$.

We thank Stephen Cowley for bringing to our attention the work described in Pugh's (1989) doctoral dissertation.

REFERENCES

ANDERSON, C. 1985 A vortex method for flows with slight density variations. *J. Comput. Phys.* **61**, 417–444.

CAFLISCH, R. E. & LOWENGRUB, J. S. 1989 Convergence of the vortex method for vortex sheets. *SIAM J. Numer. Anal.* **26**, 1060–1080.

CAFLISCH, R. E. & ORELLANA, O. F. 1986 Long time existence for a slightly perturbed vortex sheet. *Commun. Pure Appl. Maths* **39**, 807–838.

CAFLISCH, R. E. & ORELLANA, O. F. 1989 Singular solutions and ill-posedness for the evolution of vortex sheets. *SIAM J. Math. Anal.* **20**, 293–307.

CARRIER, G. F., KROOK, M. & PEARSEN, C. E. 1966 *Functions of a Complex Variable.* McGraw Hill.

CHORIN, A. J. & BERNARD, P. S. 1973 Discretisation of a vortex sheet with an example of roll-up. *J. Comput. Phys.* **13**, 423–429.

EBIN, D. 1988 Ill-posedness of the Rayleigh–Taylor and Helmholtz problems for incompressible fluids. *Commun. Partial Diff. Equat.* **13**, 1265–1295.

KRASNY, R. 1986*a* A study of singularity formation in a vortex sheet by the point-vortex approximation. *J. Fluid Mech.* **167**, 65–93.

KRASNY, R. 1986*b* Desingularization of periodic vortex sheet roll-up. *J. Comput. Phys.* **65**, 292–313.

KRASNY, R. 1987 Computation of vortex sheet roll-up in the Treffzt plane. *J. Fluid Mech.* **184**, 123–155.

MEIRON, D. I., BAKER, G. R. & ORSZAG, S. A. 1982 Analytic structure of vortex sheet dynamics. Part 1. Kelvin–Helmholtz instability. *J. Fluid Mech.* **114**, 283–298.

MOORE, D. W. 1979 The spontaneous appearance of a singularity in the shape of an evolving vortex sheet. *Proc. R. Soc. Lond.* A **365**, 105–119.

MOORE, D. W. 1981 On the point vortex method. *SIAM J. Sci. Statist. Comput.* **2**, 65–84.

PUGH, D. A. 1989 Development of vortex sheets in Boussinesq flows – formation of singularities. Ph.D. dissertation, Imperial College, London.

ROSENHEAD, L. 1931 The formation of vortices from a surface of discontinuity. *Proc. R. Soc. Lond.* A **134**, 170–192.

ROTTMAN, J. W., SIMPSON, J. E. & STANSBY, P. K. 1987 The motion of a cylinder of fluid released from rest in a cross-flow. *J. Fluid Mech.* **177**, 307–337.

SULEM, C., SULEM, P. L., BARDOS, C. & FRISCH, U. 1981 Finite time analyticity for the two and three dimensional Kelvin–Helmholtz instability. *Commun. Math. Phys.* **80**, 485–516.

SULEM, C., SULEM, P. L. & FRISCH, U. 1983 Tracing complex singularities with spectral methods. *J. Comput. Phys.* **50**, 138–161.

TRYGGVASON, G., DAHN, W. J. A. & SBEIH, K. 1991 Fine structure of vortex sheet roll-up by viscous and inviscid simulation. *Trans. ASME* I: *J. Fluids Engng* **113**, 31–36.

VOOREN, A. I. VAN DE 1980 A numerical investigation of the rolling up of vortex sheets. *Proc. R. Soc. Lond.* A **373**, 67–80.